Electronic states and doping effect of carbon in the edge-dislocation core of bcc iron

Jia-An Yan,[1] Chong-Yu Wang,[1,2] Wen-Hui Duan,[1] and Shan-Ying Wang[1]
[1]*Department of Physics, Tsinghua University, Beijing 100084, The People's Republic of China*
[2]*Chinese Center of Advanced Science and Technology (World Laboratory), Beijing 100080, The People's Republic of China*
(Received 12 July 2003; revised manuscript received 6 January 2004; published 28 June 2004)

Using the first-principles real space DMOL3 method, we investigate the electronic structure of C doped at different types of interstitial sites in the [100](010) edge dislocation core of bcc Fe. Our energetic calculations show that C has a strong segregation tendency to enter the expansion region, which is related to the lattice distortion introduced by the dislocation. We find that there exists some charge accumulations in the expansion region, resulting in unhomogeneous charge distribution in the dislocation core. Furthermore, the trapping effect on C appears at the dislocation core center. Both dislocation and C greatly affect the electronic states of Fe atoms in the dislocation core. The analysis of the electronic structure indicates that the hybridizations between C and Fe come from C 2*p* and Fe 3*d* 4*s* 4*p*. The localized effect of C-dislocation complex distinctly affects the electronic structure as well as the energy of the system.

DOI: 10.1103/PhysRevB.69.214110 PACS number(s): 61.72.Yx, 61.72.Ji, 71.15.Nc

I. INTRODUCTION

Carbon dissolved in iron plays an important role in the strength and toughness of steels, and has attracted a lot of attention for several decades until now. The interactions of C with lattice imperfections (dislocation, grain boundary, stacking fault, surface, and microcrack) dominate the influence on the mechanical properties of iron. Previous work by Cottrell and Bilby has shown that the precipitation of carbon and nitrogen from supersaturated solution in bcc iron can be greatly accelerated due to the presence of lattice distortions by cold work.[1] Cottrell and Bilby first proposed that the segregation of carbon atoms to form atmospheres around dislocations could be used to describe the yielding and strain aging of iron.[1] Much evidence has indicated that impurity atoms migrate much more rapidly along, or close to, the dislocation line than through the regular crystal lattice itself. Speich has presented indirect evidence for segregation in iron-carbon martensites based on the electrical resistivity measurements.[2] Recently, direct evidences[3,4] of carbon atom segregation to dislocations during quenching and room temperature aging of martensite have been obtained by Smith and co-workers with field ion/atom-probe microscopy.[5] They confirmed Speich's conclusion that almost 90% of the C atoms in a 0.18 at % C martensite are segregated to dislocations.

The mechanical properties of metals are governed by many extremely complex mechanisms. One of the most important factors is the structure and mobility of dislocations.[6] Large numbers of theoretical investigations of dislocations have been performed, mostly based on classical molecular dynamics (MD) simulations with embedded-atom type interatomic potentials.[7–12] However, due to the introductions of both C impurity and dislocation into a parent bcc iron, great changes of the electronic structure may be expected. A correct account of these changes apparently lies beyond the limits of such classical MD methods, while these changes may have a significant influence on the structure and energy of dislocation and can lead to qualitative changes in the usually assumed picture of dislocation motion in metals.[13] The complex interactions between C and dislocation may also have an electronic background in addition to the factor of size misfit according to the prevailing point of view.[14] As an extended defect, the inelastic region of the dislocation core can assimilate to a cylindrical pipe of radius of several lattice constants. Within the small region of dislocation core, the inner chemical bonding associated with electronic effect, may be important. Therefore, studies based on first-principles calculations are of great interest because they can provide accurate energetics and electronic structure of the C-dislocation complex, and probe the microscopic physics responsible for the macroscopic behavior. In fact, there are numerous experimental evidences showing the importance of electronic factors in the properties of dislocations and their interactions with other defects in metals.[15–17]

As much as we know, many physicists and materials scientists have recognized that the electronic structure may also play an important role in the mechanical properties of materials.[18,19] Therefore, these properties should also be investigated by quantum mechanical methods. Studies about the electronic structure of dislocations, grain boundaries, and their interactions with other defects have been performed based on first-principles calculations.[18,20–24] Woodward and Rao have recently reported the first-principles Green function boundary condition (FP-GFBC) method, which self-consistently coupled the strain field produced by a line defect to the long-range elastic field of the host lattice.[22] Within the framework of the classical Peierls-Nabarro model, Joós and Ren studied the dislocation core in silicon using the generalized stacking-fault (GSF) energies obtained from first-principles density-functional calculations.[25] The GSF energy, first introduced by Vitek,[7] can be used to determine the nonlinear atomistic restoring forces and has been widely used to study dislocation properties.[26–29] However, to our knowledge, little work has been done to study the impurity-dislocation complex based on first-principles method, while the electronic structure of solute impurity atoms within the core region may play an important role in the impurity-dislocation interactions. The underlying atomic bonding features of C and Fe may help us understand C-dislocation in-

teractions, even the diffusion and segregation of carbon to dislocations, at a fundamental level.

Due to the small radius of the C atom (0.91 Å) as compared with that of the host Fe atom (1.24 Å), C is believed to be an interstitial element in bcc bulk iron. Some theoretical studies have been performed to investigate the bonding character of dissolved interstitial carbon with Fe. C is known to enhance the bonding at grain boundaries.[30] Messmer suggested that B, C, and N form covalentlike bonds with metal atoms, whereas S forms ioniclike bonds and draws charge from the metal atoms, leading to weakening of the metal-metal bonds.[30] Hong and Anderson examined the diffusion of interstitial C atom in bcc iron using the atom superposition and electron-delocalization molecular-orbital theory.[31] They showed that interstitial C is most stably bound at a position near the octahedral site, and the diffusion barrier comes when it migrates through the octahedral site. The strong covalent bond between Fe and interstitial C results from the Fe $3d$-C $2s,2p$ hybridizations.[31,32]

In view of the importance of localized chemical bonding in addition to the long-range elastic interaction in the C-dislocation complex, we adopt a cluster model to investigate the electronic states. We present here the results of first-principles electronic structure calculations of C doped at different interstitial sites in the compression region (CR) and expansion region (ER) within the [100](010) dislocation core of bcc iron. The electronic structure of C doped at the core centers is also calculated for comparison. The outline of this paper is as follows: we briefly describe our model and computational methodology in Sec. II. In Sec. III, we present detailed results of the energetics and electronic structure of carbon doped at different interstitial sites. The results of C doped at interstitial sites in bulk Fe are also presented for comparison. We summarize our results and conclusions in Sec. IV.

II. METHOD AND MODEL

In this work, we employ the first-principles software DMOL3, a numerical cluster method based on the density functional theory (DFT),[33,34] to calculate the energetics and the electronic structure of C doped at different interstitial sites within the dislocation core of bcc Fe. DMOL3, i.e., Density functional for Molecules and three-dimensional periodic solids, has been successfully applied to calculating various systems such as molecular clusters, chemisorption, surface reconstruction, and the ground state of transition metal clusters.[35,36] For a given basis set size, DMOL3 uses the localized numerical linear combinations of atomic orbitals as basis sets to give maximum accuracy. In our calculations, a customized basis set with frozen-core approximation is used. The variational bases are $2s2p$ for C and $3d4s4p$ for Fe atom, respectively. The nonspin-polarized wave functions are used, for we are mainly concerned with the structural and mechanical properties, and the Vosko-Wilk-Nusair[37] potential is adopted as the local exchange-correlation functional.

The cluster model of Fe [100](010) edge dislocation is constructed as follows. First, we select a primary configuration by applying an elastic continuum strain field to a bcc crystal with the Burgers vector $a[100]$ (a is the lattice constant and equals 2.87 Å). Then, more than 21000 atoms with respectively 145, 31, and 16 atom layers along x, y, z directions are selected and relaxed by molecular dynamics (MD) method using the Finnis-Sinclair potential.[38] Periodic boundary condition is applied to the z direction and fixed boundary conditions to the x and y directions, respectively. The relaxation results in a configuration with near C_{2v} symmetry. From this configuration, we extract a cluster model of the dislocation core, which is illustrated in Fig. 1. The atoms denoted by solid and open circles constitute alternate (001) crystal planes (denoted as A and B, respectively) and are stacked consecutively. We can see that two nonequivalent dislocation cores are presented in planes A and B. Hence, two different core centers are formed, and will be referred to as Center-A and Center-B, respectively. To study the C-dislocation interaction, we construct two models: (i) model A, with ABABA stacking along [001] direction and totally 131 Fe atoms, and (ii) model B, with BABAB stacking and 129 Fe atoms. We have carefully tested the effect of the cluster size on the electronic structure of Fe in the dislocation core, and found that the essential features of electronic structure can be well described in the above two models without loss of significant accuracy.[39] The two cores, Center-A and Center-B, have been shown in Fig. 2.

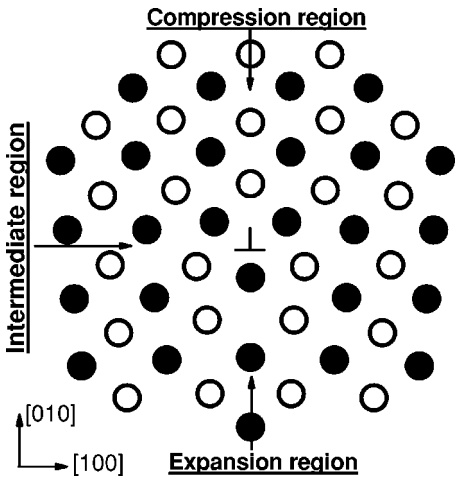

FIG. 1. Atomic model of the [100](010) edge dislocation core in bcc Fe. Atoms denoted by the black and open circles construct two adjacent planes (plane A and plane B, respectively) in the stacking sequence along [001].

The study of [100](010) edge dislocation in bcc iron, despite its simplicity, is very helpful for understanding the interactions between impurity and dislocation. In atom planes A and B, the core can be divided into three distinct regions: expansion region (ER, under the slip plane (010)), compression region (CR, above the slip plane), and intermediate region (just across the slip plane). In ER, Fe atoms are in a dilation state along the x direction, which is parallel to the slip plane. In contrast with ER, Fe atoms are extruded together in CR. To investigate the interstitial states, we select the doping models based on the following considerations: (i) interstitial space to hold carbon atom, i.e., octahedral or tetrahedral interstitial sites; (ii) local geometrical symmetry of

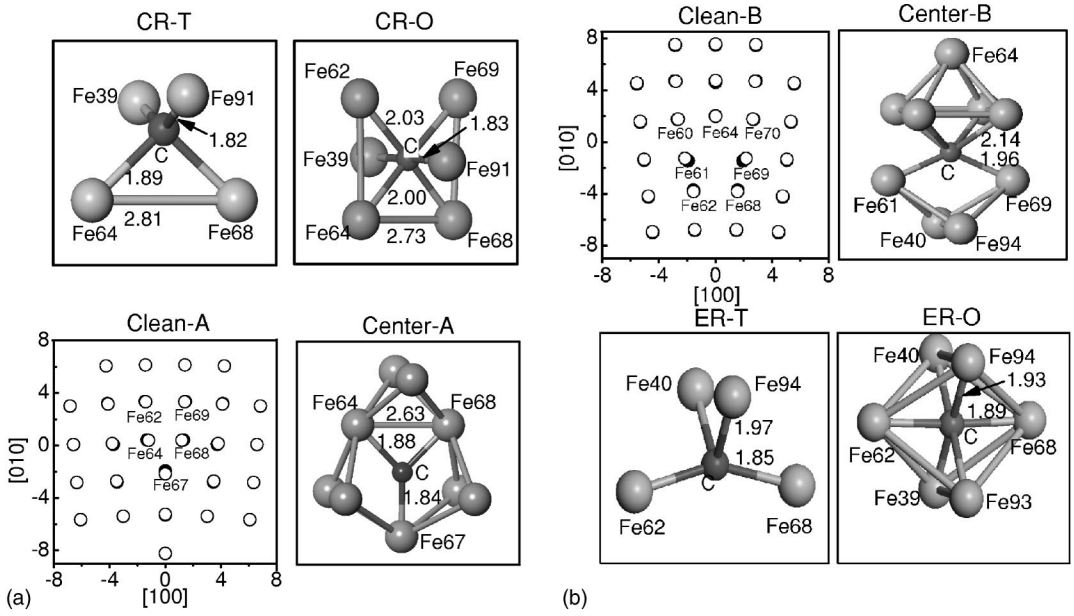

FIG. 2. Atomic models and interstitial states used in the calculations. In model A (model B), Fe atoms in the initial and the reoptimized dislocation core are shown as open circles and black circles in Clean-A (Clean-B), respectively. (a) Interstitial states CR-T, CR-O, as well as Center-A in model A; (b) ER-T, ER-O, as well as Center-B in model B. The optimized bond lengths between C and its neighboring Fe atoms are given in each case. Some Fe-Fe distances are also marked for clarity.

interstitial carbon; and (iii) stress field environment, i.e., whether the carbon is in CR or ER. We focus our study on serval typical interstitial states. As illustrated in Fig. 2, we select octahedral and tetrahedral interstitial sites from ER and CR, and denote them as ER-T, ER-O, CR-T, CR-O, respectively. Here O and T correspond to octahedral and tetrahedral sites, respectively. Center-A and Center-B are also included for the sake of comparison. Note that the tetrahedral site ER-T is next to the octahedral site ER-O, and CR-T is next to CR-O. Moreover, all the sites are selected from the middle plane of total five layers in order to minimize the boundary influence.

Assuming a very dilute solution of C in bcc iron, we consider a single impurity model. Interstitial states are studied with only one C atom doped at corresponding interstitial site within the core region. The introduction of carbon will cause significant relaxations. Therefore, we perform structure optimizations by using DMOL3 with the total energy minimization. Atoms in the top and bottom layers as well as the outermost atoms in the middle three layers are fixed during the relaxations to simulate a bulk environment. Atoms surrounding C and atoms in the dislocation core have been fully relaxed in each case. During the relaxations, C has been fixed at the interstitial site. All the optimized models are shown in Fig. 2. We use these structures to investigate the electronic states of C-dislocation complex. For octahedral cases, the centers of corresponding octahedrons are selected as the octahedral interstitial sites. The gradient convergence criterion for geometry optimization is 0.001 Ry/a.u. and the electron density convergence for self-consistent iteration is 0.00005. The electronic structure of C and surrounding Fe atoms in each case is discussed in Sec. III.

III. RESULTS AND DISCUSSIONS

To use the real-space cluster method, one must guarantee that the cluster size is large enough. Hence, we investigate the formation energies with carbon at octahedral site in bcc bulk Fe, using clusters of various numbers of Fe atoms. The clusters used have a D_{4h} point group symmetry for carbon at O site and include 6, 30, 72, and 116 Fe atoms surrounding C, respectively. For the clusters with 72 and 116 Fe atoms, up to at least the third nearest-neighbor Fe atoms of C are included. We calculate the formation energies using the definition $E_f=-(E_b^{\mathrm{dop}}-E_b^{\mathrm{clean}})$, where E_b^{dop} and E_b^{clean} are the binding energies of clusters with and without C, respectively. The obtained values are 10.06, 9.11, 9.10, and 9.21 eV, respectively. From these results, we see that while the third nearest-neighbor Fe atoms of C are included in the cluster, the obtained binding energy can be regarded as reliable, since it does not vary much (about 0.1 eV) with respect to the cluster size.

A. C at interstitial sites in bcc bulk Fe

As a comparison, we first calculate the optimized structures for C doped at interstitial octahedral (O) and tetrahedral (T) sites in bcc bulk Fe. Based on the above calculations, a cluster model of 116 Fe atoms with D_{4h} symmetry is used for C at O site. And for C at T site, we use a cluster of 108 Fe atoms with D_{2d} symmetry. Our models enable relaxations of the surrounding Fe atoms up to the third nearest-neighbor. The successive changes of gradient are less than 0.001 Ry/a.u. before we stop the optimization. During relaxations, C atom is fixed for each case. The optimized structures for C at O and T sites have been shown in Fig. 3.

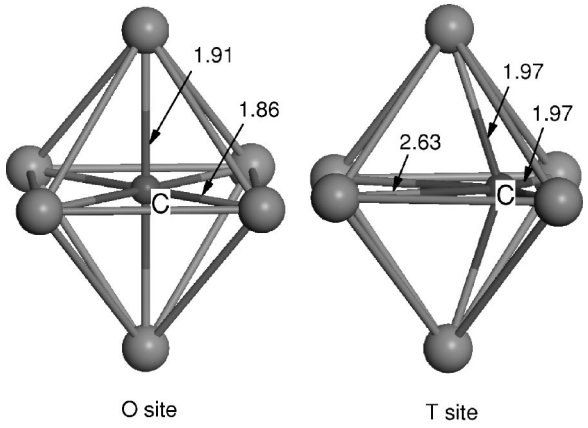

FIG. 3. Optimized structures of C doped at octahedral (O) and tetrahedral (T) sites in bcc bulk Fe. The bond lengths between C and its neighboring Fe atoms have been shown in the figure.

In the O structure, the two nearest-neighboring Fe atoms move away 0.48 Å and the four next-nearest-neighboring Fe atoms move 0.17 Å toward C from their original lattice point. The distance between C and the nearest Fe atom is 1.91 Å, in agreement with 1.89 Å obtained by Hong *et al.*[31] But the distance between C and the next-nearest-neighboring Fe atom is 1.86 Å, much smaller than 2.17 Å obtained by Hong. Our result shows a contraction of the four next-nearest-neighboring Fe atoms, which maybe results from the covalentlike bonding between C and Fe. In the T structure, four Fe atoms adjacent to C expand to a distance of 1.97 Å, consistent with 1.97 Å obtained by Hong. The calculated formation energies are 11.12 eV and 11.19 eV for C at O and T sites, respectively. The difference is less than 0.10 eV, almost negligible. This result is in well agreement with previous work by Hong *et al.*[31]

B. Clean dislocation core

The structure of dislocation core is very important due to its singularity. To compare with the core structure obtained by empirical MD method, we perform the reoptimizations of the cores by using first-principles DMOL3 method. During the relaxations the fixed atoms are the same as above mentioned in Sec. II. The reoptimized structures are shown as black circles in Clean-A and Clean-B in Fig. 2. The initial Fe positions obtained from MD method are shown as circles. We see that only slight displacements take place in the middle atomic layer in models A and B, which indicates that the structure of dislocation core obtained by MD method is reliable. We must point out that because Fe atoms in the two neighboring layers are also allowed to move in [001] direction during the relaxations, small displacements along [001] direction can be observed for these atoms. Thus, accurately speaking, the dislocation is no longer planar, which needs to be investigated further. However, we neglect these small displacements for simplicity. The reoptimizations decrease the binding energy by 2.55 eV and 3.04 eV for Clean-A and Clean-B, respectively.

To see the influence of reoptimizations on the electronic structure, we draw the local densities of states (LDOS) for Fe64 and Fe67 in Clean-A as well as Fe64 and Fe61 in Clean-B, which are regarded as the "central atoms of the dislocation core," in Figs. 4(a) and 4(b). The LDOS for bcc bulk Fe is also calculated for comparison. Many peaks exhibit on the LDOS curve for bcc bulk Fe. These evident peaks are mainly ascribed to the coordination field in bcc bulk: every Fe atom has eight nearest-neighbors with an O_h point group symmetry. However, due to the significant lattice distortions in the dislocation core, the high symmetry has been destroyed and the number of nearest-neighbors decreases. As a result, only several peaks can be observed on the LDOSs for Fe in Clean-A and Clean-B (see Fig. 4). In

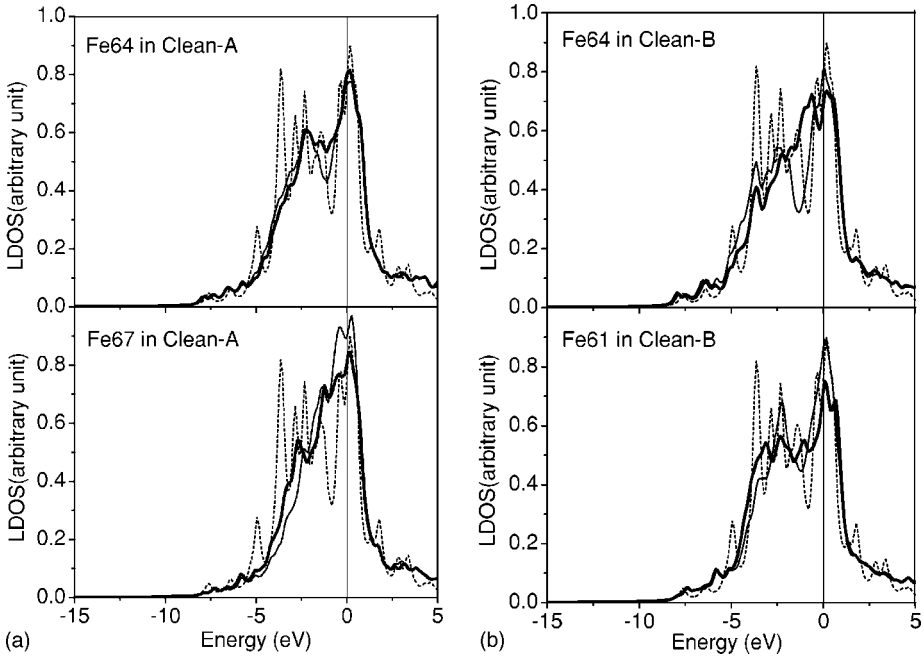

FIG. 4. LDOS for Fe64 and Fe67 in Clean-A along with LDOS for Fe64 and Fe61 in Clean-B. The Fermi energy level is shifted to zero. Thick line: after reoptimization; thin line: before reoptimization; dashed line: result for Fe in bcc bulk.

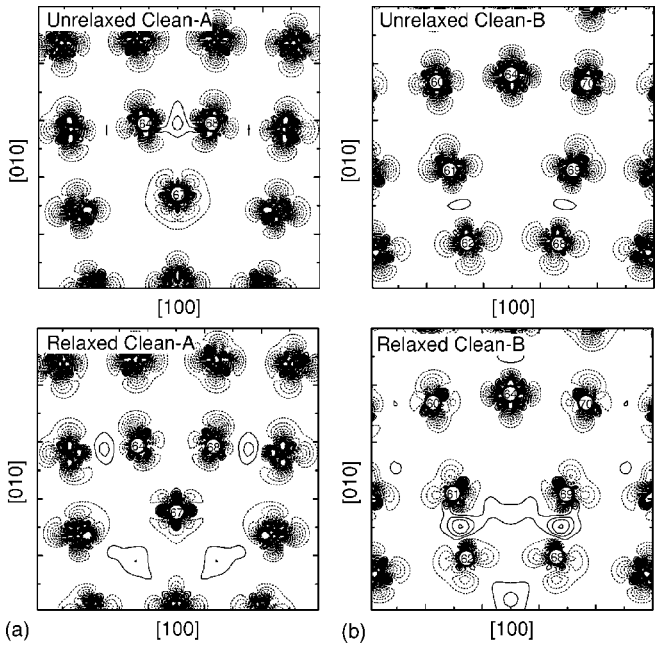

FIG. 5. Charge-density difference of Clean-A and Clean-B before and after reoptimization. The contour plots are in the middle (001) planes of model A and model B, respectively. The numbers marked in the plots correspond to Fe atoms in Fig. 2. The contour spacings are 0.0025 $e/(\text{a.u.})^3$. Solid (dashed) lines mean a gain (loss) of charge.

addition, the reoptimizations decrease the LDOS at E_F as compared with that for the initial case, indicating that some itinerant electrons in the system have been transferred to deeper inside the valence band, and giving rise to some localized electronic states. For example, a well-defined localized peak can be found at about −2.5 eV on the LDOS for Fe67 in Clean-A. Localized peaks can also be found on LDOSs for Fe64 and Fe61 in Clean-B. Another interesting phenomena is that remarkable splitting between bonding and antibonding states near E_F exhibits on the LDOS for Fe64 in Clean-B after reoptimization. On the LDOS for Fe61 in Clean-B, a weak peak above E_F can be seen in Clean-B (see Fig. 4) after reoptimization.

Charge-density differences are also shown in Figs. 5(a) and 5(b). Comparing the result of reoptimization with that of the initial case, we can observe some charge accumulations in the ER below the slip plane, both in Clean-A and Clean-B. Thus, unhomogenous charge distribution is presented in the dislocation core, which may be one of the causes of C segregation to the dislocation core.

The above analyses of LDOSs and charge-density differences show that due to the introduction of dislocation, electronic states can be significantly affected in contrast to those in bcc bulk.

C. C at interstitial sites in the dislocation core

In this section, we present the energetics and electronic structure of C doped at different interstitial sites in the two dislocation cores: Clean-A and Clean-B.

1. Energy analysis

We define the impurity segregation energy as

$$E_{\text{seg}} = \frac{E_b^{\text{dop}} - E_b^{\text{clean}}}{N}, \tag{1}$$

where N is the total number of impurity atoms in the C-doped system. E_b^{dop} is the binding energy of the C-doped system, while E_b^{clean} the binding energy of the clean system. The binding energy of a cluster is defined as $E_b = E_t - E_a$, where E_t is the total energy of the cluster and E_a is the sum of free atomic total energies. Table I shows the segregation energies E_{seg} for each interstitial state. Segregation energy can be used to reflect the local effects of the impurity atoms on a system. The calculation results of segregation energies indicate that C will prefer to enter the core center and expansion region rather than the compression region. In the expansion region, the segregation energy of ER-T is lower than that of ER-O by about 0.40 eV. This shows that when C migrates from a tetrahedral site to a second tetrahedral site through an octahedral site, an energy barrier must be surmounted.

Table I shows that E_{seg} of all interstitial states in ER are lower than those in CR, by at least 0.20 eV. The main causes are the atomic environment and the state of corresponding stress field. Due to the dilatation in ER, the distance of two neighboring Fe atoms is longer than that in CR, which makes larger interstitial space for C. For example, the bond length of C-Fe68 in ER-O is 1.89 Å, almost 3.3% longer than that of C-Fe91 in CR-O (1.83 Å). Therefore, the stress field caused by the lattice distortions will affect the preference of C's occupying sites. Our calculations of segregation energy show that C atom will prefer to occupy the interstitial sites in expansion region, which is in accord with classical analysis.[40,41]

From Table I, we can see that Center-B has the lowest segregation energy in all cases. The result indicates that Center-B is the most stable state, showing the strong complex effects between C and dislocation core. The trapping effect of the core center on C atom will probably influence the dislocation mobility. As a result, the dislocation may be

TABLE I. Calculated segregation energy E_{seg} for each interstitial state (Unit: eV).

	Core center		Compression region		Expansion region	
	Center-A	Center-B	CR-T	CR-O	ER-T	ER-O
E_{seg}	−9.20	−9.84	−9.02	−9.04	−9.62	−9.22

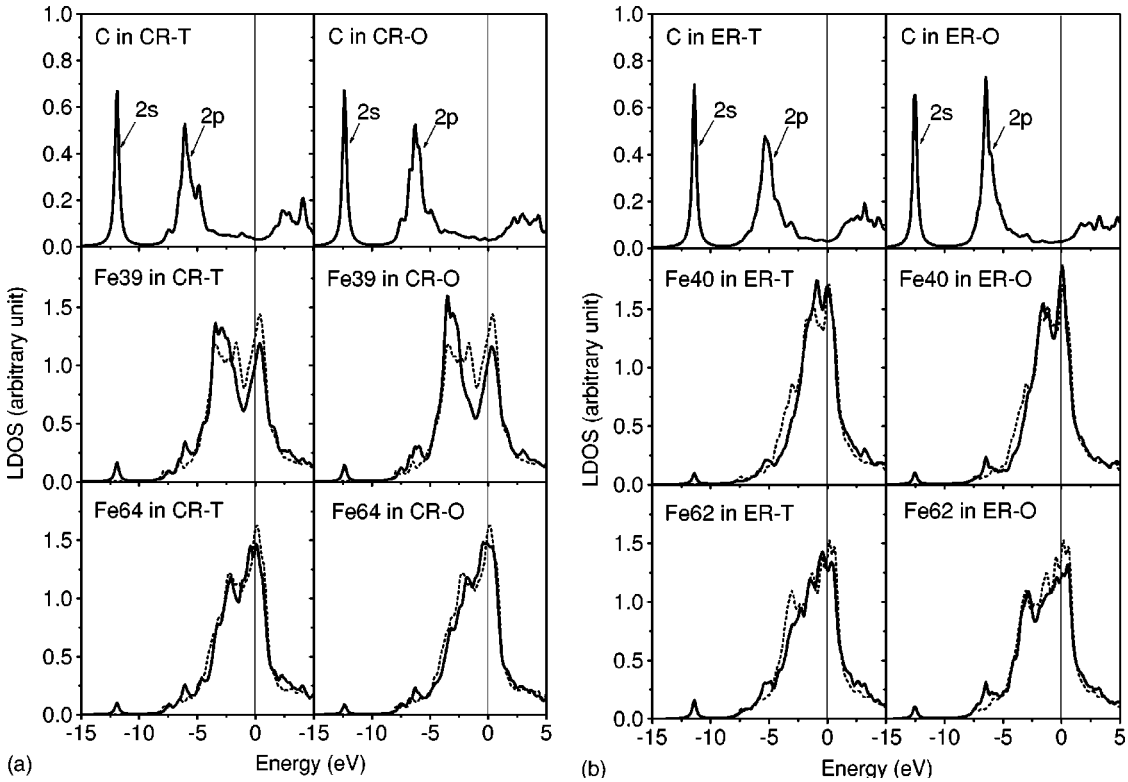

FIG. 6. LDOS for C and its neighboring Fe atoms in (a) CR-T and CR-O, (b) ER-T and ER-O. The solid and dashed lines correspond to with and without C at the interstitial sites, respectively. The Fermi energy level is shifted to zero.

pinned, which will affect the macroscopic mechanical properties of iron.

2. Density of states

The local densities of states (LDOS) are closely related to the bonding character between atoms. Considering the local symmetry around the C atom, we only draw LDOSs for the nonequivalent Fe atoms neighboring to C.

In Fig. 6(a), the LDOSs for the C atom and the neighboring Fe39, Fe64 in CR-T and CR-O are presented. The C 2*s* band, which occurs as a single, well-defined peak at about 12.0 eV below E_F, undergoes relatively small interaction with any of the Fe bands. The C 2*p* band exhibits a peak structure over a range about 4–7 eV below E_F. These peaks, dominated by the 2*p* component, overlap with Fe states near the bottom of the valence bands, consistent with strong bonding interactions of C and Fe. The C 2*p* band exhibits a broad distribution of states over the entire conduction band region up to 5 eV above E_F. The presence of the C atom has a marked effect upon the LDOS curves for the neighboring Fe39 and Fe64 atoms, indicating mixing of C 2*p* states with Fe 3*d*4*s*4*p* states. There is also a remarkable increase of the splitting between bonding and antibonding states near E_F on the LDOSs for Fe39 in both CR-T and CR-O, which is an indication of the increase of hybridization between Fe39 and C. A well-defined peak lies at just above E_F, and a localized peak appears at about 3.0 eV below E_F, suggesting the formation of localized state. In contrast, the splitting is not so evident on the LDOS for Fe64. In fact, referring to Fig. 2, we see that the bond lengths of C-Fe39 are 1.82 Å in CR-T and 1.83 Å in CR-O, less than those of C-Fe64 by 0.07 Å in CR-T and 0.17 Å in CR-O, respectively. Thus, it is natural that Fe39 shows much stronger hybridization with C.

In Fig. 6(b), the LDOSs for C atom and the neighboring Fe40, Fe62 in ER-T and ER-O are presented. The C 2*s* 2*p* bands are similar to those in Fig. 6(a). However, a relative narrowing of Fe bands can be observed, especially on the LDOSs for Fe40, as compared with the LDOSs for Fe39 and Fe64 in both CR-T and CR-O. In addition, there is also a little splitting of bonding and antibonding states near E_F on the LDOSs for Fe40 and Fe62, but the splitting is not so strong as that for Fe39 in CR-T and CR-O. These differences can be illustrated with the different bond length of C and Fe. Referring to ER-T and ER-O models in Fig. 2, we see that in the case of ER-T, the distance between C and Fe40 is 1.97 Å, much longer than 1.82 Å for C-Fe39 in CR-T. Therefore, the hybridization of C with Fe40 in ER-T is not so strong as that of C with Fe39 in CR-T.

Figure 7 shows the LDOSs for C atom and the neighboring Fe atoms in Center-A and Center-B. In the cases of Center-A and Center-B, we see that C 2*p* bands now exhibit two or more distinct peaks ranging over about 4–7 eV below E_F, suggesting that there is a distortion of bonds of C and Fe. This is consistent with the charge distribution analysis to be discussed below. Due to the large distortion in the dislocation core, not only bond length but also bond angle of the σ-type bonding between C-2*p* and Fe atomic orbitals will be greatly distorted, as clearly shown in Fig. 8. As in Fig. 6, the C 2*p* bands also extend over a broad energy range up to 5 eV above E_F. This character indicates the strong hybridization of C-2*p* with the neighboring Fe states.

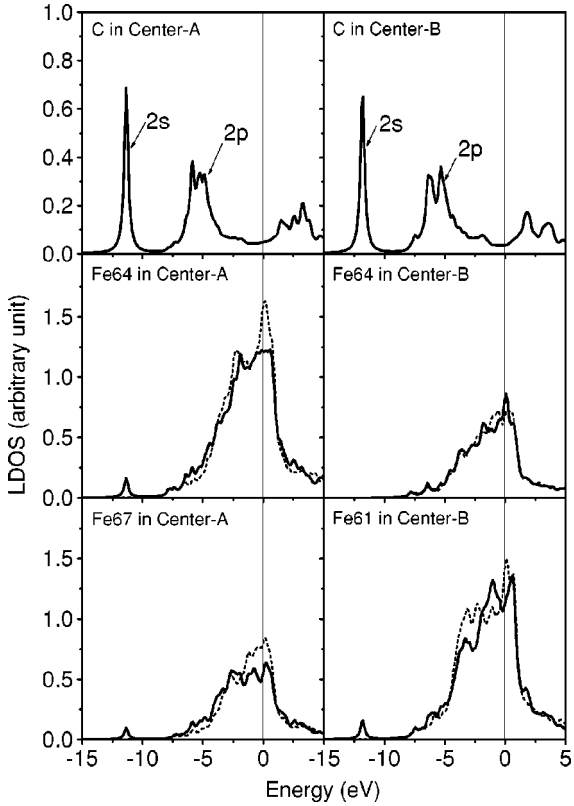

FIG. 7. LDOS for C and its neighboring Fe atoms in Center-A and Center-B. The solid and dashed lines correspond to with and without C at the interstitial sites, respectively. The Fermi energy level is shifted to zero.

From Figs. 6 and 7, we see a remarkable decrease of the LDOS at E_F for the neighboring Fe atoms, in comparison with the calculated LDOS for the clean system. This means that some itinerant electrons are transferred to some deeper energy level in the valence band, and participate in the bonding with C. Detailed analysis of partial density of states (PDOS) indicates that the chemical bonding between C and Fe can mainly attribute to the hybridization of C $2p$ with Fe $3d$ $4s$ $4p$.

It can be seen that many of the LDOS curves presented have peaks or upward trends near the Fermi level. This suggests that the details of the electronic structure may vary with temperature (note: it is at finite temperature that the motivating phenomena occur). It should be pointed out that our calculations are not involved with temperature (i.e., $T=0$ K are implied). However, the analysis should also be qualitatively applicable to finite temperature cases.

The location of the Fermi energy is of great interest because it is closely connected with many macroscopic physical properties of metals, especially transport (electroconductivity, thermopower, etc.) properties, magnetic properties, and so on. It is very notable that the Fermi energy level lies at different locations on the LDOS for Fe atoms. When a distinct peak appears at just above the Fermi energy level, it indicates that the Fe atom is easy to obtain some more electrons. This will greatly affect the electrical conductivity of the system. From the different locations of the Fermi energy level in Figs. 6 and 7, we can infer that impurity-dislocation

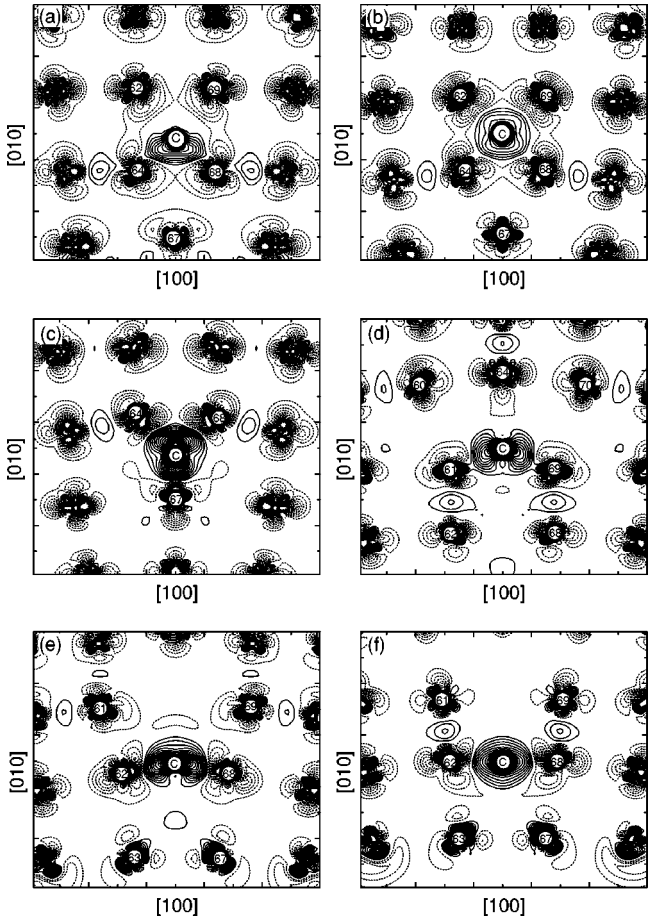

FIG. 8. Charge-density difference of interstitial states. The contour plots are in a plane containing carbon and its neighboring Fe atoms. The numbers marked in (a)–(f) correspond to Fe atoms shown in Fig. 2. The contour spacings are $0.0025e/(\text{a.u.})^3$. Solid (dashed) lines mean a gain (loss) of charge. (a) CR-T; (b) CR-O; (c) Center-A; (d) Center-B; (e) ER-T; (f) ER-O.

complex will affect some macroscopic physical properties of metals such as electroconductivity in addition to the usual mechanical properties.

3. Charge distribution

Figure 8 shows the charge-density difference in the (001) plane containing C and serval neighboring in-plane Fe atoms for each interstitial state. The charge-density difference is calculated by subtracting free atomic charge density from the charge density of the carbon at each interstitial site, so that the carbon-induced charge redistribution can be seen clearly. From Fig. 8, pronounced charge redistributions can be observed for all interstitial states. The strong chemical bonding between C and the neighboring Fe atoms is evident. A common feature is that the interactions between C and Fe atoms are localized to a small region near the impurity, for all interstitial states. This verifies our assumption of the local effect of C-dislocation complex.

In tetrahedral sites CR-T and ER-T [Figs. 8(a) and 8(e)], the charge accumulates mainly between C and its tetrahedral neighboring Fe atoms. In addition, some distortions of the

TABLE II. Mülliken populations of valence orbitals of C and its neighboring Fe atoms in each interstitial state. Q is the summation of the populations in valence orbitals of atom. In bcc bulk Fe, the calculated populations of 3*d*, 4*s*, and 4*p* are 6.501, 0.405, and 1.127, respectively, and Q is 8.033.

		Model A						Model B			
		Clean-A	Center-A	CR-T	CR-O			Clean-B	Center-B	ER-T	ER-O
C	2*s*		1.465	1.442	1.421	C	2*s*		1.429	1.458	1.415
	2*p*		3.051	3.209	3.272		2*p*		3.178	3.177	3.287
	Q		4.516	4.651	4.693		*Q*		4.607	4.635	4.702
Fe39	3*d*	6.524	6.521	6.540	6.539	Fe40	3*d*	6.528	6.524	6.540	6.545
	4*s*	0.456	0.483	0.455	0.462		4*s*	0.444	0.463	0.430	0.395
	4*p*	1.255	1.283	1.217	1.254		4*p*	1.005	0.998	0.857	0.946
	Q	8.235	8.017	8.212	8.255		*Q*	7.977	7.985	7.827	7.886
Fe64	3*d*	6.514	6.523	6.528	6.528	Fe61	3*d*	6.513	6.522	6.518	6.514
	4*s*	0.410	0.355	0.372	0.355		4*s*	0.419	0.353	0.392	0.415
	4*p*	1.076	1.044	0.885	0.946		4*p*	1.148	1.080	1.075	1.099
	Q	8.000	7.922	7.785	7.829		*Q*	8.080	7.955	7.985	8.028
Fe67	3*d*	6.513	6.522	6.514	6.515	Fe62	3*d*	6.513	6.505	6.533	6.526
	4*s*	0.393	0.368	0.411	0.395		4*s*	0.387	0.392	0.338	0.324
	4*p*	0.989	1.061	0.977	0.973		4*p*	1.080	1.161	0.961	1.043
	Q	7.895	7.951	7.902	7.884		*Q*	7.980	8.058	7.832	7.893

C-Fe bond can be seen. For octahedral interstitial states, the shape of the contours suggests that C form σ-type bonding state with the two nearest Fe atoms [Fe62 and Fe68 in Fig. 8(f)].

In Center-A, the charge accumulation between C and its three nearest Fe atoms is very evident in Fig. 8(c), while in Center-B, C only forms bonds with Fe61 and Fe69, as shown in Fig. 8(d). In each case, C obtains some charge and neighboring Fe atoms lose some charge, consistent with Mülliken charge transfer analysis to be discussed below.

4. Mülliken analysis

Mülliken analysis can give us many details about charge transfer.[42] Table II gives the Mülliken populations of valence orbitals of C and its neighboring Fe atoms in each interstitial state. The populations of Fe 3*d*, 4*s*, and 4*p* in bcc bulk as well as in clean dislocations (Clean-A and Clean-B) are also calculated and listed in Table II. Obviously, C obtains electrons by about 0.60 *e* in all cases, while Fe loses some electrons, so the charge transfer is just from Fe to C.

We first compare the populations of Fe in clean dislocation with those in bulk. According to our calculations, the populations of 3*d*, 4*s*, and 4*p* of bcc bulk Fe are 6.501, 0.405, and 1.127, respectively, and the summation Q is 8.033. The result indicates that some 4*s* electrons have been transferred to 4*p* and 3*d*. The total charge of Fe67 in Clean-A is less than that of bcc bulk Fe by 0.14 *e*, while the Q of Fe39 in Clean-A is 8.235, by about 0.20 *e* more than that of bcc bulk Fe. These changes can be also verified from charge-density differences in Fig. 5. The results show that the lattice distortions introduced by dislocation can greatly affect the charge transfer, consequently, the hybridizations of Fe atoms.

When a C atom is introduced into interstitial sites in dislocation core, for example, at Center-A and Center-B, C will obtain electrons from its neighboring Fe atoms and form covalentlike bonds [see Figs. 8(c) and 8(d)]. As compared with the case of Clean-A, the charge summation Q for Fe39 and Fe67 decreases by about 0.22 *e* and 0.05 *e* in Center-A, respectively. In Center-B, Fe61 loses 0.13 *e* as compared with that in Clean-B. Meanwhile, the summation of charge Q of C in Center-A is less than that in CR-T and CR-O, by about 0.15 *e*, and the most of charge transfer comes from C 2*p*. This can be ascribed to the strong hybridizations of C-2*p* with the electronic states of neighboring Fe atoms in both CR-T and CR-O. In addition, C has only three nearest-neighbor Fe atoms compared with four in CR-T and six in CR-O. From charge transfer analysis, we see that C strongly hybridizes with Fe atoms in the dislocation core. As a result, the energy and electronic structure are greatly changed.

IV. SUMMARY

In summary, we have performed first-principles calculation of C doped at different interstitial sites in the compres-

sion and expansion regions as well as core centers within the [100](010) edge dislocation core of bcc Fe. The calculations of segregation energy show that C will prefer to enter the expansion region and core centers rather than the compression region. Furthermore, the trapping effect on C appears at the center of the dislocation core (Center-B).

As compared with that of bcc bulk Fe, the electronic structure of Fe atoms is greatly changed due to the distortions in the dislocation core. Splitting between bonding and antibonding states near E_F has been observed in the LDOS. Furthermore, some charge accumulations appear in the expansion region. The introduction of C to the dislocation core significantly affects energetics as well as the electronic structure of Fe atoms in the core. The analysis of the electronic structure of C and its nearest Fe atoms shows that the hybridization of Fe 3*d* 4*s* 4*p* with C 2*p* are related to the localized states as well as the covalent bonding character.

However, the impurity-dislocation interaction in metals is very complex. Much more systematic studies should be performed in order to clarify the underlying microscopic mechanisms of the dislocation-impurity complex.

ACKNOWLEDGMENTS

This work was supported by "973" Project from the Ministry of Science and Technology of China (Grant No. G2000067102) and National Natural Science Foundation of China (Grant No. 59801009).

[1] A. H. Cottrell, *Effect of Solute Atoms on the Behavior of Dislocations*, in Proceedings of the Conference on Strength of Solids, Bristol, 7–9 July 1947, edited by N. F. Mott (The Physical Society, London, 1948), pp. 30–38; A. H. Cottrell and B. A. Bilby, Proc. Phys. Soc., London, Sect. A **62**, 49 (1949).
[2] G. R. Speich, Trans. Soc. Min. Eng. AIME **245**, 2553 (1969).
[3] M. K. Miller, P. A. Beaven, and G. D. W. Smith, Metall. Trans. A **12A**, 1197 (1981).
[4] L. Chang, S. J. Barnard, and G. D. W. Smith, in *Fundamentals of Aging and Tempering in Bainitic and Martensitic Steel Products*, edited by G. Krauss and P. E. Repas (ISS-AIME, Warrendale, PA, 1992), p. 19.
[5] J. Wilde, A. Cerezo, and G. D. W. Smith, Scr. Mater. **43**, 39 (2000).
[6] M. S. Duesbery, in *Dislocations in Solids*, edited by F. R. N. Nabarro (North-Holland, Amsterdam, 1989), Vol. 8, p. 67.
[7] V. Vitek, Prog. Mater. Sci. **36**, 1 (1992).
[8] D. Farkas, C. G. Schon, M. S. F. Delima, and H. Goldenstein, Acta Mater. **44**, 409 (1996).
[9] A. Béré and A. Serra, Phys. Rev. B **65**, 205323 (2002).
[10] Q. F. Fang and R. Wang, Phys. Rev. B **62**, 9317 (2000).
[11] J. Chang, W. Cai, V. V. Bulatov, and S. Yip, Comput. Mater. Sci. **A309-310**, 160 (2001).
[12] J. Chang, W. Cai, V. V. Bulatov, and S. Yip, Comput. Mater. Sci. **23**, 111 (2002).
[13] S. Ismail-Beigi and T. A. Arias, Phys. Rev. Lett. **84**, 1499 (2000).
[14] P. Haasen, *Physical Metallurgy*, edited by R. W. Cahn and P. Haasen (North-Holland, Amsterdam, 1996).
[15] M. Molotskii and V. Fleurov, Phys. Rev. Lett. **78**, 2779 (1997).
[16] V. I. Altshits, E. V. Darinskaya, and O. L. Kazakova, Zh. Eksp. Teor. Fiz. **111**, 615 (1997) [JETP **84**, 338 (1997)].
[17] Yu. I. Golovin, R. B. Mogutnov, A. A. Baskakov, and M. V. Badylevich, Pis'ma Zh. Eksp. Teor. Fiz. **69**, 114 (1999) [JETP Lett. **69**, 127 (1999)].
[18] R. Wu, A. J. Freeman, and G. B. Olson, Science **265**, 376 (1994).
[19] S.-H. Jhi, J. Ihm, S. G. Louie, and M. L. Cohen, Nature (London) **399**, 132 (1999).
[20] O. Yu. Kontsevoi, Yu. N. Gornostyre, A. J. Freeman, M. I. Katsnelson, and A. V. Trefilov, Philos. Mag. Lett. **81**, 455 (2001), and references therein.
[21] J. X. Shang and C. Y. Wang, Phys. Rev. B **66**, 184105 (2002).
[22] C. Woodward and S. I. Rao, Phys. Rev. Lett. **88**, 216402 (2002).
[23] Y. N. Gornostyrev, M. I. Katsnelson, N. I. Medvedeva, O. N. Mryasov, A. J. Freeman, and A. V. Trefilov, Phys. Rev. B **62**, 7802 (2000).
[24] N. Kioussis, M. Herbranson, E. Collins, and M. E. Eberhart, Phys. Rev. Lett. **88**, 125501 (2002).
[25] B. Joós, Q. Ren, and M. S. Duebery, Phys. Rev. B **50**, 5890 (1994).
[26] V. V. Bulatov and E. Kaxiras, Phys. Rev. Lett. **78**, 4221 (1997).
[27] J. Hartford, B. von Sydow, G. Wahnström, and B. I. Lundqvist, Phys. Rev. B **58**, 2487 (1998).
[28] O. N. Mryasov, Yu. N. Gornostyrev, and A. J. Freeman, Phys. Rev. B **58**, 11927 (1998).
[29] G. Lu, N. Kioussis, V. V. Bulatov, and E. Kaxiras, Phys. Rev. B **62**, 3099 (2000).
[30] R. P. Messmer and C. L. Briant, Acta Metall. **30**, 457 (1982).
[31] Sung Y. Hong and A. B. Anderson, Phys. Rev. B **40**, 7508 (1989).
[32] M. Morinaga, N. Yukawa, H. Adachi, and T. Mura, J. Phys. F: Met. Phys. **17**, 2147 (1987).
[33] P. C. Hohenberg and W. Kohn, Phys. Rev. **136**, B864 (1964).
[34] W. Kohn and L. J. Sham, Phys. Rev. **140**, A1133 (1965).
[35] B. Delley, J. Chem. Phys. **92**, 508 (1990).
[36] B. Delley, J. Chem. Phys. **94**, 7245 (1991).
[37] S. H. Vosko, L. Wilk, and M. Nusair, Can. J. Phys. **58**, 1200 (1980).
[38] M. W. Finnis and J. E. Sinclair, Philos. Mag. A **50**, 45 (1984); **53**, 161(E) (1986).
[39] To test the influence of cluster size on the electronic structure, we added one more outer shell of Fe atoms to the cluster and calculated the LDOS for C and Fe62 in ER-O. Only a slight change can be seen in comparison with the result obtained here. From this, we infer that our cluster model can be used without loss of significant accuracy.
[40] J. Friedel, *Dislocations* (Pergamon Press, Oxford, 1964).
[41] J. P. Hirth and J. Lothe, *Theory of Dislocations* (Wiley, New York, 1982).
[42] R. S. Mülliken, J. Chem. Phys. **23**, 1833 (1955).